The Astrophysical Journal, 826:132 (6pp), 2016 August 1 doi:10.3847/0004-637X/826/2/132

J1216+0709: A RADIO GALAXY WITH THREE EPISODES OF AGN JET ACTIVITY

Veeresh Singh[1], C. H. Ishwara-Chandra[2], Preeti Kharb[3], Shweta Srivastava[1], and P. Janardhan[1]
[1] Astronomy & Astrophysics Division, Physical Research Laboratory, Ahmedabad 380009, India
[2] National Centre for Radio Astrophysics, TIFR, Post Bag 3, Ganeshkhind, Pune 411007, India
[3] Indian Institute of Astrophysics, II Block, Koramangala, Bangalore 560034, India
Received 2016 March 16; revised 2016 May 18; accepted 2016 May 18; published 2016 July 27

ABSTRACT

We report the discovery of a "triple-double radio galaxy," J1216+0709, detected in deep low-frequency Giant Metrewave Radio Telescope (GMRT) observations. J1216+0709 is only the third radio galaxy, after B0925+420 and Speca, with three pairs of lobes resulting from three different episodes of active galactic nucleus (AGN) jet activity. The 610 MHz GMRT image clearly displays an inner pair of lobes, a nearly coaxial middle pair of lobes, and a pair of outer lobes that is bent with respect to the axis of the inner pair of lobes. The total end-to-end projected sizes of the inner, middle, and outer lobes are 40″ (∼95 kpc), 1.′65 (∼235 kpc), and 5.′7 (∼814 kpc), respectively. Unlike the outer pair of lobes, both the inner and middle pairs of lobes exhibit asymmetries in arm lengths and flux densities, but in the opposite sense, i.e., the eastern sides are farther and also brighter than the western sides, thus, suggesting the possibility of the jet being intrinsically asymmetric rather than due to a relativistic beaming effect. The host galaxy is a bright elliptical ($m_r \sim 16.56$) with $M_{SMBH} \sim 3.9 \times 10^9\ M_\odot$ and a star formation rate of $\sim 4.66^{+4.65}_{-1.61}\ M_\odot\ yr^{-1}$. The host galaxy resides in a small group of three galaxies ($m_r \leqslant 17.77$) and is possibly going through an interaction with faint dwarf galaxies in the neighborhood, which may have triggered the recent episodes of AGN activity.

Key words: galaxies: active – galaxies: individual (J1216+0709) – galaxies: jets – radio continuum: galaxies

1. INTRODUCTION

Radio galaxies, a subclass of active galactic nuclei (AGNs), are powerful radio emitters and typically exhibit radio morphology that consists of a core producing a pair of bipolar collimated jets terminating in the form of lobes. Therefore, detection of "core-jet-lobe" radio morphology is a clear indication of AGN activity. In fact, radio morphological structure and spectral properties can be used to probe the history of AGN activity. Morphological studies of radio galaxies have been useful in understanding the precession or change of jet axis in X-shaped radio galaxies, the effect of the motion of host galaxies in bent radio galaxies, and intermittent AGN activity in radio galaxies showing two pairs of lobes (Dehghan et al. 2014; Roberts et al. 2015). In recent years, there have been attempts to understand the details of recurrent AGN activity in galaxies by studying radio galaxies exhibiting two pairs of lobes that are formed during two different phases of AGN activity (e.g., Jamrozy et al. 2009; Konar et al. 2013). These galaxies are generally termed as "double-double radio galaxies (DDRGs)," in which a new pair of radio lobes is seen closer to nucleus, before the distant and old pair of radio lobes fades away (Saikia & Jamrozy 2009). The new pair of lobes is edge brightened; therefore, it can easily be distinguished from knots in the jets.

Interestingly, despite the identification of thousands of radio galaxies in various radio surveys, only a few dozen are confirmed DDRGs (Nandi & Saikia 2012), possibly due to lack of sensitivity and resolution such that radio structures at different spatial scales remain undetected. Low-frequency sensitive Giant Metrewave Radio Telescope (GMRT) observations with the resolution of a few arcseconds are well suited to detect both steep-spectrum, low-surface-brightness radio emission from the old pair of lobes and kiloparsec-scale emission from the new pair of lobes.

In this paper we report the discovery of a rare "triple-double radio galaxy (TDRG)," J1216+0709, that displays three pairs of lobes in the 610 MHz GMRT image. This is only the third TDRG reported so far, after B0925+420 (Brocksopp et al. 2007) and Speca (Hota et al. 2011). This radio galaxy is either undetected or poorly detected in previous radio surveys (e.g., Faint Images of the Radio Sky at Twenty-cm [FIRST], Becker et al. 1995; NRAO VLA Sky Survey [NVSS], Condon et al. 1998; VLA Low-frequency Sky Survey [VLSS], Cohen et al. 2007; TIFR-GMRT Sky Survey [TGSS], Intema et al. 2016) due to the lack of optimum sensitivity and resolution. The host galaxy has been identified in the Sloan Digital Sky Survey (SDSS; Ahn et al. 2014) as an early-type galaxy at R.A. (J2000) = $12^h\,16^m\,32.^s42$ and decl. (J2000) = +07°09′55.″8 with a spectroscopically measured redshift $z = 0.136$.

The cosmological parameters that we adopt are $H_0 = 71$ km s^{-1} Mpc^{-1}, $\Omega_M = 0.27$, and $\Omega_{vac} = 0.73$. Using this cosmology, 1″ corresponds to 2.381 kpc at the luminosity distance of ∼633.8 Mpc for J1216+0709.

2. GMRT OBSERVATIONS AND DATA REDUCTION

The radio galaxy J1216+0709 was observed with the GMRT at 610 MHz on 2012 June 20 and at 325 MHz on 2016 April 23. During our GMRT observations, we used the full array of 30 antennas and the software backend with receiver bandwidth of 32 MHz subdivided into 256 channels. During the 610 MHz observations, the target field centered at NGC 4235 (R.A. (J2000) = $12^h17^m09.^s9$ and decl. = +07°11′30″) was observed for nearly 4 hr, whereas in 325 MHz observations the field was centered on the target source J1216+0709 and was observed for nearly 3.5 hr. The amplitude calibrators were observed for ∼20 minutes at the start and/or end of each run, and the phase calibrators were observed for ∼5 minutes every ∼40 minutes. GMRT data

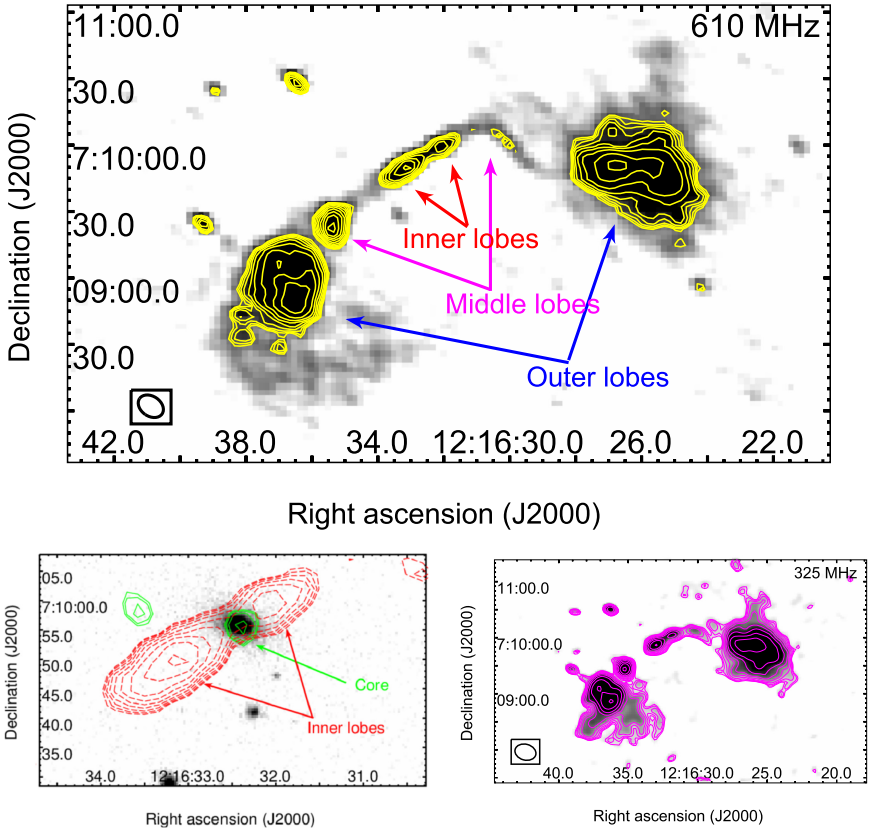

Figure 1. Top panel: 610 MHz image displaying three pairs of lobes. For better visualization of different lobes the contours represent only bright emission, with the lowest contour at the $>6\sigma$ level. Bottom left panel: zoom-in view of the 610 MHz contours of the inner lobes and 1.4 GHz FIRST-detected core (in green) overlaid on the SDSS *r*-band image. Bottom right panel: 325 MHz GMRT image, with contours overlaid onto the gray scale. Contours are spaced in logarithmic scale, with the lowest contour at the 5σ level. The synthesized elliptical beam enclosed in a rectangular box is shown at the bottom left corner.

were reduced and analyzed in the standard way using the NRAO Astronomical Image Processing System (AIPS). Calibrated visibilities were Fourier transformed to create radio images by using the "IMAGR" task and a robust weighing scheme, where the robust parameter was set to "0" (between uniform and natural weighing) at both frequencies. All the images were self-calibrated and primary beam corrected. Our final maps have noise rms $\sim 40\ \mu$Jy beam^{-1} with a synthesized beam size of $\sim 6\farcs2 \times 4\farcs5$ at 610 MHz, and $\sim 160\ \mu$Jy beam^{-1} with a synthesized beam size of $\sim 11\farcs4 \times 8\farcs5$ at 325 MHz. More details on the data reduction are presented in Kharb et al. (2016). The total flux densities of different components were measured using the AIPS task "TVSTAT," which allows us to choose an area of any shape. Error on the flux density of a component was obtained by multiplying the average noise rms by the total area of the component measured in units of synthesized beams. Flux density of an individual component was obtained by considering the area shown by contours overlaid on the grayscale image.

3. RADIO PROPERTIES

3.1. Radio Morphology

J1216+0709 is best imaged at 610 MHz in GMRT observations, while it is either undetected or poorly detected in existing radio surveys. The 610 MHz GMRT image displays an inner pair of lobes, a nearly coaxial middle pair of lobes, and a pair of outer lobes that are bent with respect to the inner pair of lobes (see Figure 1). The overall radio morphology of the source appears bent in a "C"-shaped structure and resembles somewhat a wide angle tail (WAT) radio galaxy. The total end-to-end projected sizes of the inner lobes, middle lobes, and outer lobes are $40''$ (~95 kpc), $1\farcm65$ (~235.7 kpc), and $5\farcm7$ (~814 kpc), respectively (see Figure 1). The three distinct pairs of lobes can be interpreted as evidence for the three different episodes of AGN jet activity. The inner and middle pairs of lobes show clear edge-brightened structures that distinguish them from knots in the jets. In the 610 MHz image, there is relatively faint bridge-like radio emission connecting the two successive lobes, which tentatively indicates that the newly formed jets propagate outward possibly through the jet-cocoon structure formed by the previous episode of activity rather than through the intergalactic medium.

Radio flux densities of different components at different frequencies are given in Table 1. Based on the 610 MHz image, Table 2 lists total radio sizes, ratios of flux densities, and arm lengths of the eastern and western side lobes and the luminosities of the three pairs of lobes. We note that for the outer pair of lobes, both eastern and western lobes have similar flux densities and distance from the center (i.e., arm lengths), which suggests that the outer pair of lobes is lying nearly in the plane of sky. For both the inner and middle pairs of lobes, the eastern side is nearly 2.3–2.5 times stronger than the western side, i.e., ratios of flux densities of the eastern to western lobe for inner and middle pairs are $(R_{\rm f,in}) \sim 2.3$ and $(R_{\rm f,mid}) \sim 2.5$, respectively (see Table 2). Also, for both the inner and middle pairs of lobes, the arm lengths of the eastern sides are larger than those of the western sides, i.e., the ratios of eastern to

Table 1
Radio Properties

Parameter	$S_{\rm int,325\ MHz}$ (mJy)	$S_{\rm int,610\ MHz}$ (mJy)	$S_{\rm int,1.4\ GHz}$ (mJy)	$\alpha_{325\,\rm MHz}^{610\,\rm MHz}$	$\alpha_{610\,\rm MHz}^{1.4\,\rm GHz}$
Inner lobe (E)	8.2 ± 0.8	5.2 ± 0.5	...	-0.72 ± 0.06	...
Inner lobe (W)	3.8 ± 0.6	2.3 ± 0.4	...	-0.80 ± 0.10	...
Middle lobe (E)	11.9 ± 1.2	8.4 ± 0.6	...	-0.55 ± 0.05	...
Middle lobe (W)	5.4 ± 1.5	3.7 ± 1.8	...	-0.60 ± 0.24	...
Outer lobe (E)	75 ± 11.5	47.9 ± 13.8	20.0 ± 1.4	-0.71 ± 0.14	-1.05 ± 0.13
Outer lobe (W)	100 ± 12	55.8 ± 19.6	21.3 ± 1.5	-0.92 ± 0.16	-1.16 ± 0.16
Total	207 ± 32	125 ± 14.6	51.5 ± 2.4	-0.80 ± 0.08	-1.07 ± 0.05
Core	$<0.48 \pm 0.16$	$<0.12 \pm 0.04$	0.45 ± 0.2	...	$>+1.59 \pm 0.24$

Note. Outer lobe flux densities at 1.4 GHz are only crude estimates based on the area covered by the outer lobe seen in the 610 MHz image. There is no clear detection of an AGN core in the 325 and 610 MHz images, and hence we use a 3σ lower limit at these frequencies.

Table 2
Radio Sizes and Luminosities

$l_{\rm in}$ (kpc)	$l_{\rm mid}$ (kpc)	$l_{\rm out}$ (kpc)	$R_{\rm l,in}$	$R_{\rm l,mid}$	$R_{\rm l,out}$	$R_{\rm f,in}$	$R_{\rm f,mid}$	$R_{\rm f,out}$	$P_{\rm in,610\ MHz}$ (W Hz^{-1})	$P_{\rm mid,610\ MHz}$ (W Hz^{-1})	$P_{\rm out,610\ MHz}$ (W Hz^{-1})	$P_{\rm total,610\ MHz}$ (W Hz^{-1})
95	235	814	2.0	1.6	1.0	2.28	2.5	0.85	3.5×10^{23}	5.4×10^{23}	4.8×10^{24}	5.8×10^{24}

Note. $l_{\rm in}$, $l_{\rm mid}$, and $l_{\rm out}$ represent total end-to-end linear sizes of inner, middle, and outer pairs of lobes, respectively. $R_{\rm l,in}$, $R_{\rm l,mid}$, and $R_{\rm l,out}$ are ratios of the linear sizes of eastern to western sides of the inner, middle, and outer pairs of lobes, respectively. $R_{\rm f,in}$, $R_{\rm f,mid}$, and $R_{\rm f,out}$ are 610 MHz flux density ratios of eastern to western lobes for the inner, middle, and outer pairs of lobes, respectively. $P_{\rm in,610\ MHz}$, $P_{\rm mid,610\ MHz}$, and $P_{\rm out,610\ MHz}$ are 610 MHz luminosities of the inner, middle, and outer pairs of lobes, respectively. The radio luminosities are k-corrected by assuming that the radio emission is synchrotron emission characterized by a power law ($S\nu \propto \nu^{\alpha}$), where we use the spectral index value measured between 325 and 610 MHz. The radio luminosity of the source at redshift z and luminosity distance $d_{\rm L}$ is, therefore, given by $P\nu = 4\pi d_{\rm L}^2\ S\nu\ (1+z)^{-(\alpha+1)}$.

western sides are $(R_{\rm l,in}) \sim 2.0$ to $(R_{\rm l,mid}) \sim 1.6$, for the inner and middle pair, respectively. We note that the asymmetry shown by inner and middle doubles in our source is consistent with the general trend found in DDRGs in which the inner doubles tend to be more asymmetric in both its arm length and its flux density ratios compared to the outer doubles (see Saikia et al. 2006). It is worth noting that for both inner and middle doubles the asymmetries in arm lengths and flux densities are in the opposite sense, i.e., the eastern lobes are farther and also brighter than the western lobes. The opposite asymmetry is difficult to explain by a simple version of the relativistic beaming effect. Also, in radio galaxies the viewing angle is relatively large (>45°; Urry & Padovani 1995); therefore, the relativistic beaming effect is unlikely to be dominant. This strengthens the possibility of the jet being intrinsically asymmetric. Indeed, an asymmetric jet has been suggested for some of the DDRGs reported in the literature (see Jamrozy et al. 2009). In our TDRG the outer pair of lobes is bent with respect to the axis of the inner pair of lobes, and this can be understood if the outer lobes are entraining into a medium having large-scale density gradients or the host galaxy has moved during the two cycles of AGN activity (Kantharia et al. 2009). The 610 MHz radio luminosities of the inner, middle, and outer pairs of lobes are 3.5×10^{23} W Hz^{-1}, 5.4×10^{23} W Hz^{-1}, and 4.8×10^{24} W Hz^{-1}, respectively (see Table 2). The higher luminosity of the outer pair of lobes in comparison to the inner pair of lobes is consistent with other cases of TDRGs and DDRGs (see Schoenmakers et al. 2000). The total 610 MHz radio luminosity (5.8×10^{24} W Hz^{-1}) of our TDRG (with r-band absolute magnitude $M_{\rm R} \sim -20.69 \pm 0.03$; Simard et al. 2011) is close to the separation line between FR I and FR II types (Fanaroff & Riley 1974). Interestingly, the western outer lobe with edge brightening is similar to FR II, while the eastern one bears resemblance to an FR I type.

We note that there is no clear detection of the AGN core in both the 610 and 325 MHz images, whereas the core is marginally detected in the FIRST image at the 2σ level (~0.45 mJy). Since our 610 MHz images have a typical noise rms of 0.04 mJy, this gives an upper limit of core flux density of 0.12 mJy at the 3σ level. Therefore, the AGN radio core exhibits an inverted spectral index between 610 MHz and 1.4 GHz (see Table 1). The compact inverted-spectrum AGN core is similar to gigahertz-peaked spectrum sources (GPSs) that exhibit a peak in their radio spectra between 1 and 5 GHz and an inverted-shape spectrum at lower frequencies (Fanti 2009). GPSs are interpreted as radio AGNs in early phases of their evolution; therefore, compact inverted-spectrum radio cores of TDRGs may be considered as an indication of recent AGN activity (Randall et al. 2011; Orienti 2016). Indeed, some DDRGs are known to show a mildly inverted spectrum of the core (Machalski et al. 2010).

3.2. Radio Spectrum

Figure 2 shows spectral index maps between 610 MHz and 1.4 GHz and between 325 and 610 MHz. We use the task "COMB" in AIPS to create spectral index images after considering flux density values above 2.5σ at both frequencies. The resolutions of the images at two frequencies were matched by convolving the higher-resolution image with a Gaussian equivalent to the beam size of the lower-resolution image. A spectral index map between 610 MHz (GMRT) and 1.4 GHz (NVSS) shows that the outer lobes have a steeper spectral index ($\alpha \sim -1.0$, where $S_\nu \propto \nu^{\alpha}$), while the inner region (covering the core and inner lobes) has relatively less steep spectral index ($\alpha > -0.5$). The 325–610 MHz spectral index map is of higher

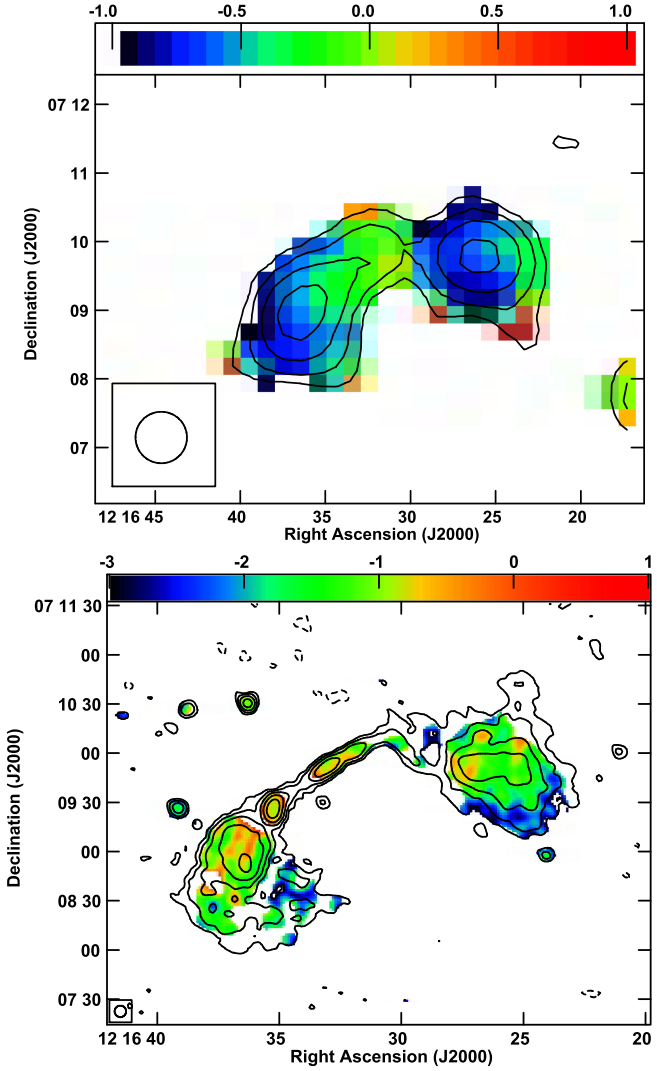

Figure 2. Top panel: spectral index map between 610 MHz (GMRT) and 1.4 GHz (NVSS) with NVSS contours overlaid onto it. Bottom panel: spectral index map between 325 and 610 MHz with 610 MHz contours overlaid onto it.

spatial resolution and shows all three lobes. We note that, in the 325–610 MHz spectral index map, the outer lobes have a steeper spectral index ($\alpha \leqslant -1.0$) in comparison to the inner and middle lobes. Also, outer edges of the outer lobes have a very steep spectral index ($\alpha \leqslant -2.0$), which is typically seen in relic plasma. There is no signature of relatively compact hot-spot-like structures with a less steep spectral index, therefore suggesting that the supply of jet material stopped long ago and hot spots in the outer lobes have completely faded away, if they existed.

3.3. Kinematic Age Estimates

It is important to estimate the timescales of active and quiescent phases of AGN activity to understand the cause of episodic AGN activity and its duty cycle. Given the lack of multifrequency radio data for our TDRG, we can only constrain the lower limit to the active and quiescent phase timescales by using kinematic age estimates based on projected radio sizes and a reasonable assumed value for the jet speed. We note that, in general, for a constant jet power the advancement speed of the head of the lobe is higher at an early phase of evolution and decreases (via interaction with the surrounding medium) as the source size increases (An & Baan 2012). Based on the previous studies of both young and evolved radio galaxies, we adopt the average speed of the advancement of the head of outer, middle, and inner lobes of our source to be $0.01c$, $0.05c$, and $0.1c$, respectively (where c is the speed of light; see Konar et al. 2006; Machalski et al. 2010; An et al. 2012). With these assumed speeds and projected linear sizes of ~814, ~235, and ~95 kpc for the outer, middle, and inner doubles, respectively, we obtain kinematic ages of $\sim 1.3 \times 10^8$ yr, $\sim 7.6 \times 10^6$ yr, and $\sim 1.5 \times 10^6$ yr for the outer, middle, and inner doubles, respectively. However, we caution that our estimates of kinematic ages are only an order-of-magnitude approximation under the simplified assumption that the advancement speed of the lobe remains constant. We also attempt to put a constraint on the timescale of the quiescent phase between the two AGN episodes. The duration of the quiescent phase is equivalent to the time interval between the last jet material being injected into the outer lobes and the first jet material being ejected from AGNs in the next episode. The time elapsed since the last injection of relativistic particles in the jet can be estimated by a synchrotron aging method, which requires modeling of the radio spectrum to obtain a break frequency that is related to the age of the synchrotron-emitting plasma. Due to the lack of multifrequency radio data necessary for spectral modeling, we can only place a lower limit on the quiescent phase timescale (t_q) by subtracting the kinematic ages of outer ($t_{\text{out-lobe}}$) and inner doubles ($t_{\text{in-lobe}}$), i.e., $t_q \leqslant t_{\text{out-lobe}} - t_{\text{in-lobe}}$. Therefore, the quiescent phase timescales between outer (first episode) and middle (second episode) doubles and the middle (second episode) and inner (third episode) are $\leqslant 1.2 \times 10^8$ yr and $\leqslant 6.1 \times 10^6$ yr, respectively. These limits on the quiescent phase timescales are consistent with the timescale estimates in DDRGs (see Konar et al. 2013). Our proposed multifrequency GMRT and VLA observations will allow us to put much stronger constraints on the timescales via spectral aging measurements.

4. HOST GALAXY AND ITS LARGE-SCALE ENVIRONMENT

A host galaxy and its surrounding large-scale environment can play a crucial role in triggering episodic AGN activity; therefore, we examine the nature of the host galaxy and its environment. Radio contours overlaid on the SDSS optical image identify the host galaxy as an elliptical galaxy at a redshift of ~0.136 (see Figure 1). The host galaxy is fairly bright (r-band magnitude $\simeq$16.56) and redder in color ($u - r = 2.89$). The SDSS optical spectrum is dominated by a red continuum with a noticeable 4000 Å break, characteristic of early-type galaxies. The optical emission line flux ratio diagnostic classifies the host galaxy as a low-excitation radio galaxy. The *Wide-field Infrared Survey Explorer* (*WISE*; Wright et al. 2010) colors of the host galaxy ([3.4]–[4.6] = 0.12 < 0.8 in Vega magnitudes) indicate that the mid-IR emission is dominated by star formation and that AGN contamination is not significant (see Stern et al. 2012). We estimate a star formation rate (SFR) of $\sim 4.66^{+4.65}_{-1.61}\ M_\odot\ \text{yr}^{-1}$ in the host galaxy using the Kennicutt (1998) empirical relation (SFR ($M_\odot\ \text{yr}^{-1}$) = $4.5 \times 10^{-44}\ L_{8-1000\ \mu\text{m}}$ (erg s^{-1})) based on IR luminosity. The total IR (8–1000 μm) luminosity is estimated from the *WISE* 22 μm luminosity using the full range of templates in the libraries of Chary & Elbaz (2001) and Dale

& Helou (2002). For our TDRG we estimate the mass of the supermassive black hole ($M_{\rm SMBH}$) to be $\sim 3.87 \times 10^9\ M_\odot$ by using the "black hole mass–bulge luminosity" relation for early-type galaxies given in McConnell & Ma (2013). The absolute bulge magnitude of our source is taken from Simard et al. (2011), who present bulge–disk decomposition for SDSS DR7 galaxies. To examine whether our TDRG is associated with any cluster or group, we use the catalog of Tempel et al. (2014), who identified galaxy groups and clusters based on a modified friends-of-friends method and present a flux ($m_{\rm r} \leqslant 17.77$) and volume-limited catalog using SDSS DR 10 data. The value of the flux limit is based on the fact that the SDSS data are incomplete for fainter sources (Strauss et al. 2002). According to the Tempel et al. (2014) catalog, the host galaxy is part of a small group of three galaxies (other two galaxies located at R.A. (J2000) = $12^{\rm h}16^{\rm m}39^{\rm s}$, decl. (J2000) = $+07°10'25''$ and R.A. (J2000) = $12^{\rm h}16^{\rm m}30^{\rm s}$, decl. (J2000) = $+07°06'14''$) with a total estimated mass of $\sim 1.99 \times 10^{13}\ M_\odot$ and a virial radius of ~0.28 Mpc.

There is no apparent disturbance in the host galaxy morphology, and thus we can rule out any recent major merger. However, a minor merger or a strong interaction with a dwarf galaxy is plausible without resulting in any prominent disturbance. In the SDSS image, two faint, blue-color, dwarf-galaxy-like objects (one at R.A. (J2000) = $12^{\rm h}16^{\rm m}31\overset{\rm s}{.}97$, decl. (J2000) = $+07°09'47\overset{''}{.}28$ with $m_{\rm r} \sim 23.31 \pm 0.27$ but without any estimate of redshift due to faintness, and a second one at R. A. (J2000) = $12^{\rm h}16^{\rm m}32\overset{\rm s}{.}25$, decl. (J2000) = $+07°09'40\overset{''}{.}92$ with $m_{\rm r} \sim 19.67 \pm 0.02$ and $z_{\rm phot} \sim 0.118 \pm 0.0402$) are seen close to the southern side of the TDRG host galaxy. The apparent fuzziness and blue color may be an indication of a strong interaction that might have triggered a recent star formation. So, it is possible that both these dwarf galaxies are interacting with the TDRG host galaxy, which can bring sufficient matter close to the SMBH to trigger AGN activity. However, more sensitive optical observations are required to obtain spectroscopic redshifts of these dwarf galaxies and to confirm this possibility.

5. SUMMARY

We report the discovery of a rare "TDRG," J1216+0709, that exhibits three distinct pairs of lobes in the 610 MHz GMRT image. This TDRG is only the third such source reported, after B0925+420 and Speca, where three pairs of lobes are the result of three different episodes of AGN jet activity. The 610 MHz GMRT image exhibits an inner pair of lobes, a nearly coaxial middle pair of lobes, and a pair of outer lobes that are bent with respect to the inner pair of lobes. The total end-to-end projected sizes of the inner double, middle double, and outer double are 40″ (~95 kpc), 1.′65 (~235.7 kpc), and 5.′7 (~814 kpc), respectively. We note that unlike the outer pair of lobes, both the inner and middle doubles exhibit asymmetries in arm lengths and flux densities but in the opposite sense, i.e., the eastern sides are farther and also brighter than the western sides. The opposite asymmetry is difficult to explain by a simple version of the relativistic beaming effect and suggests the possibility of the jet being intrinsically asymmetric. Also, all three pairs of lobes bear an edge-brightened resemblance with FR II type radio galaxies, while their total radio luminosities are lower than that for classical FR II radio galaxies. A spectral index map between 325 and 610 MHz shows that the outer lobes exhibit a steeper spectral index ($\alpha \leqslant -1$) in comparison to the middle and inner lobes. The lack of hot spots and a very steep spectral index in the outer edges of outer lobes indicate the presence of relic plasma.

Kinematic age estimates based on assumed advancement speeds of the heads of the lobes of $0.01c$, $0.05c$, and $0.1c$ for the outer, middle, and inner doubles, respectively, are $\sim 1.3 \times 10^8$ yr, 7.6×10^6 yr, and 1.5×10^6 yr for the outer, middle, and inner pair of lobes, respectively. The kinematic age estimates allow us to put a lower limit on the quiescent phase timescales between outer (first episode) and middle (second episode) doubles, and the middle (second episode) and inner (third episode) doubles to be $\leqslant 1.2 \times 10^8$ yr and $\leqslant 6.1 \times 10^6$ yr, respectively. The host galaxy is found to be a bright elliptical (r-band magnitude ~16.56) for which the optical spectrum is dominated by a red continuum and emission-line ratios suggest AGN emission to be of low excitation. The host galaxy contains an SMBH with a mass of $\sim 3.87 \times 10^9$ and SFR $\sim 4.66^{+4.65}_{-1.61}\ M_\odot\ {\rm yr}^{-1}$. Also, the host galaxy belongs to only a small group of three galaxies, with a total estimated mass of the group of $\sim 1.99 \times 10^{13}\ M_\odot$ and a virial radius of ~0.28 Mpc. There is no apparent disturbance in the morphology of the host galaxy; however, it may be interacting with two nearby dwarf galaxies. So, the AGN activity might have been triggered by the interaction with neighboring dwarf galaxies. However, more sensitive optical data are required to confirm this plausibility.

The GMRT is a national facility operated by the National Centre for Radio Astrophysics of the Tata Institute of Fundamental Research. We thank the staff at NCRA and GMRT for their support. This research has made use of the NASA/IPAC Extragalactic Database (NED), which is operated by the Jet Propulsion Laboratory, California Institute of Technology, under contract with the National Aeronautics and Space Administration. This publication makes use of data products from *WISE*, which is a joint project of the University of California, Los Angeles, and the Jet Propulsion Laboratory/California Institute of Technology, funded by the National Aeronautics and Space Administration. Funding for SDSS-III has been provided by the Alfred P. Sloan Foundation, the Participating Institutions, the National Science Foundation, and the US Department of Energy Office of Science. The SDSS-III website is http://www.sdss3.org/. SDSS-III is managed by the Astrophysical Research Consortium for the Participating Institutions of the SDSS-III Collaboration, including the University of Arizona, the Brazilian Participation Group, Brookhaven National Laboratory, Carnegie Mellon University, University of Florida, the French Participation Group, the German Participation Group, Harvard University, the Instituto de Astrofisica de Canarias, the Michigan State/Notre Dame/JINA Participation Group, Johns Hopkins University, Lawr ence Berkeley National Laboratory, Max Planck Institute for Astrophysics, Max Planck Institute for Extraterrestrial Physics, New Mexico State University, New York University, Ohio State University, Pennsylvania State University, University of Portsmouth, Princeton University, the Spanish Participation Group, University of Tokyo, University of Utah, Vanderbilt University, University of Virginia, University of Washington, and Yale University.

REFERENCES

Ahn, C. P., Alexandro, R., Allende Prieto, C., et al. 2014, ApJS, 211, 17
An, T., & Baan, W. A. 2012, ApJ, 760, 77
An, T., Wu, F., Yang, J., et al. 2012, ApJS, 198, 5
Becker, R. H., White, R. L., & Helfand, D. J. 1995, ApJ, 450, 559
Brocksopp, C., Kaiser, C. R., Schoenmakers, A. P., et al. 2007, MNRAS, 382, 1019
Chary, R., & Elbaz, D. 2001, ApJ, 556, 562
Clarke, D. A., & Burns, J. O. 1991, ApJ, 369, 308
Cohen, A. S., Lane, W. M., Cotton, W. D., et al. 2007, AJ, 134, 1245
Condon, J. J., Cotton, W. D., Greisen, E. W., et al. 1998, AJ, 115, 1693
Dale, D. A., & Helou, G. 2002, ApJ, 576, 159
Dehghan, S., Johnston-Hollitt, M., Franzen, T. M. O., et al. 2014, AJ, 148, 75
Fanaroff, B. L., & Riley, J. M. 1974, MNRAS, 167, 31
Fanti, C. 2009, AN, 330, 120
Hota, A., Sirothia, S. K., Ohyama, Y., et al. 2011, MNRAS, 417, L36
Intema, H. T., Jagannathan, P., Mooley, K. P., et al. 2016, arXiv:1603.04368
Jamrozy, M., Saikia, D. J., & Konar, C. 2009, MNRAS, 399, L141
Joshi, S. A., Nandi, S., Saikia, D. J., et al. 2011, MNRAS, 414, 1397
Kantharia, N. G., Das, M., & Gopal-Krishna 2009, JApA, 30, 37
Kennicutt, R. C., Jr. 1998, ARA&A, 36, 189
Kharb, P., Srivastava, S., Singh, V., et al. 2016, MNRAS, 459, 1310
Komissarov, S. S., & Gubanov, A. G. 1994, A&A, 285, 27
Konar, C., Hardcastle, M. J., Jamrozy, M., et al. 2012, MNRAS, 424, 1061
Konar, C., Hardcastle, M. J., Jamrozy, M., et al. 2013, MNRAS, 430, 2137
Konar, C., Saikia, D. J., Jamrozy, M., et al. 2006, MNRAS, 372, 693
Machalski, J., Jamrozy, M., & Konar, C. 2010, A&A, 510, A84
McConnell, N. J., & Ma, C.-P. 2013, ApJ, 764, 184
Murgia, M., Parma, P., Mack, K.-H., et al. 2011, A&A, 526, A148
Nandi, S., & Saikia, D. J. 2012, BASI , 40, 121
Orienti, M. 2016, AN, 337, 9
Polatidis, A. G. 2009, AN, 330, 149
Randall, K. E., Hopkins, A. M., Norris, R. P., et al. 2011, MNRAS, 416, 1135
Roberts, D. H., Cohen, J. P., Lu, J., et al. 2015, ApJS, 220, 7
Saikia, D. J., & Jamrozy, M. 2009, BASI , 37, 63
Saikia, D. J., Konar, C., & Kulkarni, V. K. 2006, MNRAS, 366, 1391
Schoenmakers, A. P., de Bruyn, A. G., Rottgering, H. J. A., et al. 2000, MNRAS, 315, 371
Simard, L., Mendel, J. T., Patton, D. R., et al. 2011, ApJS, 196, 11
Stern, D., Assef, R. J., Benford, D. J., et al. 2012, ApJ, 753, 30
Strauss, M. A., Weinberg, D. H., Lupton, R. H., et al. 2002, AJ, 124, 1810
Tempel, E., Tamm, A., Gramann, M., et al. 2014, A&A, 566, A1
Urry, C. M., & Padovani, P. 1995, PASP, 107, 803
Wright, E. L., Eisenhardt, P. R. M., Mainzer, A. K., et al. 2010, AJ, 140, 1868